UNIVERSITY
OF TRENTO

DIPARTIMENTO DI INGEGNERIA E SCIENZA DELL'INFORMAZIONE

38123 Povo – Trento (Italy), Via Sommarive 14
http://www.disi.unitn.it

CRACK DETECTION IN LOSSY TWO-DIMENSIONAL STRUCTURES BY MEANS OF A MICROWAVE IMAGING APPROACH

S. Caorsi, M. Donelli, M. Pastorino, and F. Righini

January 2000

Technical Report # DISI-11-096

Crack Detection in Lossy Two-Dimensional Structures by means of a Microwave Imaging Approach

Salvatore Caorsi*, Andrea Massa**, Matteo Pastorino***, and Fabio Righini***

*Department of Electronics,

University of Pavia, Via Ferrata 1, 27100 Pavia - Italy

Tel. +39 0382 505661, Fax +39 0382 422583, E-mail: *caorsi@ele.unipv.it*

**Department of Civil and Environmental Engineering,

University of Trento, Via Mesiano 77, 38050 Trento -Italy

Tel. +39 0461 882623, Fax +39 0461 882672, E-mail: *andrea.massa@ing.unitn.it*

***Department of Biophysical and Electronic Engineering,

University of Genoa, Via Opera Pia 11/A, 16145 Genoa -Italy

Tel. +39 010 3532796, Fax +39 010 3532245, E-mail: *pastorino@dibe.unige.it*

Crack Detection in Lossy Two-Dimensional Structures by means of a Microwave Imaging Approach

Salvatore Caorsi*, Andrea Massa**, Matteo Pastorino***, and Fabio Righini***

Abstract

The purpose of this paper is to present a microwave imaging approach for the determination of the position, the orientation and dimensions of a crack located inside a lossy dielectric host medium. The inversion procedure is based on a genetic algorithm which allows to iteratively generate a sequence of trial solutions minimizing a suitable cost function. The dependence of the performances of the proposed microwave imaging approach on the conductivity value of the host medium is checked. Moreover, the robustness of the algorithm to operate with noisy data is evaluated. Finally, the reconstruction of an irregular crack is considered.

1 Introduction

The use of interrogating microwaves for inspecting dielectric materials or conducting structures coated by dielectrics has been proposed from long time. However, microwave tomographic techniques are relatively news in this field.

In this paper we propose an approach for data inversion in tomographic imaging which can be of interest in the light of nondestructive evaluation (NDE) applications. The usually proposed diffraction tomography aims at reconstructing an "image" of the object under test, e.g. a pixel matrix (usually, two-dimensional imaging is performed) in which each pixel corresponds to a discretization cell (whose dimensions essentially determine the system resolution) [1].

At microwave frequencies, the scattering mechanisms must be taken into account in the reconstruction procedure. Consequently, diffraction tomography is much more complex than classical CT approaches based on approximations (e.g., straight ray propagation). The complexity results in a large computational load, mainly in terms of CPU time, for the data inversion and the image formation [1].

However, in NDE areas [2], [3], [4], the generation of a complete image of the target is not always required. The object is usually known and what is of interest is only a defect in the known cross section. The inspection process should accurately localize, orientate and shape the defect. At microwave frequencies, the inverse problem that must be solved is a highly nonlinear one. The possibility of multiple solutions may result in false localizations or artifacts that can be very problematic in several applications.

Stochastic optimization procedures [5], [6], [7] seem to be able to reach the "global" solution of the problem. Consequently, they are potential inversion tools. Procedures of this kind (in particular the genetic algorithms (GAs)) have previously been proposed for microwave imaging purposes [8]. Nevertheless, their main drawback is the computational time required to achieve the solution when many unknowns must be determined. In the microwave imaging framework, this problem is overcame by hybridizing the GA-based

procedure with a deterministic method (see for example [8], [9], [10] and the references therein). In NDE applications, the number of unknowns considerably reduces and the search space can be limited by imposing some deterministic constraints arising from the *a-priori* knowledge on the problem at hand.

It should be noted that a number of approaches based on the use of GAs has been already proposed in the NDE field. These approaches are mainly concerned with the detection of cracks by using eddy current techniques. For example, a classic binary-coded GA has been in [11], where the interaction of the exciting ECT coil with arbitrary shape cracks (parallel with each other and perpendicular to the surface of an infinite non-ferromagnetic conductor plate) is calculated by using integral equation. A constrained GA associated with a finite-element modeling for solving 2D inverse problems in ECT has been also proposed in [12]. Moreover, a numerical example of crack detection using a probe that can operate from DC to medium frequency has been presented in [13], in which a finite element method is used for the direct problem solution and a GA is applied as inversion tool. A process monitoring system has been developed in [14] for cold heading applications. In that work, a GA has been used to select the small subset of waveform features necessary to develop a robust artificial neural network for the differentiation among cold head machine conditions. Another evolutionary algorithm has been considered in [15] for solving the electromagnetic NDE inverse problem consisting in finding the position, dimension, categories, type, shape or number of flaws in a conducting sample starting from the information obtained by a ECT probe. Since a high number of degrees of freedom are present in the choice of the parameters governing these kind of algorithm, paper [15] is a preliminary attempt to use a meta-algorithm aiming to find the best values for the operator parameters. Essentially, this meta-algorithm is a GA having as population a set of evolutionary algorithms.

2 Mathematical Formulation

In Figure 1, a classic tomographic configuration is represented. An incident wave is generated by the transmitting antenna and impinges on the object to be inspected. To deal with a two-dimensional scalar problem, the incident wave is assumed to be transverse magnetic (TM_z) with the electric field vector polarized in the same direction of the axis of the cylindrical object. Generally, the aim is to inspect the cross-section of the cylinder, which is assumed to be homogeneous only in the z direction. A set of probes is located around the object. The measurement probes and the transmitting antenna jointly rotate around the object in order to collect multiview information (the use of multiview processing is of fundamental importance in inverse problems, as it results in a reduction of the ill-conditioning).

At microwave frequencies, there is a complicated relationship between measured data and spatial distributions of dielectric parameters of the object under test. This relationship mathematically models the laws of the e.m. scattering and can be written as [16], [17]:

$$E_{scatt}^{v,m} = E_{meas}^{v,m} - E_{inc}^{v,m} = \Im^{v,m}\{\tau\} \tag{1}$$

where:

- $E_{scatt}^{v,m}$: scattered field (z-component) at point m ($m = 1, ..., M$) for the v-th view ($v = 1, ..., V$);
- $E_{meas}^{v,m}$: measured electric field;
- $E_{inc}^{v,m}$: incident electric field;
- τ: object function defined as $\tau = (\varepsilon - 1) - j\frac{\sigma}{2\pi f \varepsilon_0}$ being ε and σ the dielectric permittivity and conductivity of the cross section (in general, inhomogeneous quantities), respectively;

- $\Im^{v,m}$: first-order Fredholm operator having as kernel the Hankel function of second kind and zero order [16];

- M, V: numbers of measurement probes and views.

In imaging applications [1], the target is the reconstruction of the object function in the whole cross-section. If highly contrasted bodies are to be inspected, "inverting" (1) results in a cumbersome and complex nonlinear inverse problem.

However, in many NDE applications, the problem is the detection of a defect in an otherwise known object (τ_{object}). In this paper, we explore the possibility of identifying the position, the orientation and the size of a crack (for simplicity approximated with a void rectangle) in the original structure. The crack is characterized by: L (length), w (width), θ (orientation), (x_0, y_0) coordinates of the center (Figure 1). The parameters L, w, and θ, are assumed to belong to finite sets: $L \in \{L_j, j = 1, ..., \Gamma\}$, $w \in \{w_i, i = 1, ..., \omega\}$ and $\theta \in \{p\Delta\theta, p = 1, ..., \Upsilon\}$. The unknowns constitute an array $\underline{\xi}$. The reconstruction problem is then to minimize the following functional:

$$\phi\left\{\underline{\xi}\right\} = \gamma_1 \sum_{m=1}^{M} \sum_{v=1}^{V} \left| E_{scatt}^{v,m} - \Im^{v,m}\left\{\underline{\xi}\right\} \right|^2 +$$

$$\gamma_2 \sum_{n=1}^{N} \sum_{v=1}^{V} \left| E_{inc}^{v,n} - \Im_0^{v,n}\left\{\underline{\xi}\right\} \right|^2 \tag{2}$$

where:

- $E_{inc}^{v,n}$: incident electric field at the center of the n-th pixel (the original cross section is partitioned into N square pixels);

- $\Im_0^{v,n}$: the operator corresponding to the Volterra equation relating the internal fields (the so called *state* equation) [17];

- γ_1, γ_2: regularization constants.

By using (2), the original inverse problem is recast into a global optimization problem. Since $\Im_0^{v,n}$ and $\Im^{v,m}$ contain as unknown also the internal total electric field, one can use the first order Born approximation [18] ($\overline{E}_{tot} \approx \overline{E}_{inc}$ inside the cross section). Since the Born approximation is not able to deal with strong scatterers [19], $\overline{E}_{tot} = E_{tot,z}\hat{z}$ is assumed here to be an unknown, and the values $E_{tot}^{v,n}$, $n = 1, ..., N$, $v = 1, ..., V$ are enclosed in the array $\underline{\xi}$.

The minimization of $\phi\left\{\underline{\xi}\right\}$ (relation (2)) is obtained by using a GA. The GA evolves a set of trial arrays, called a *population* of *individuals*, $\Omega = \{\underline{\xi}_l; l = 1, ..., L_\Omega\}$, toward the global minimum of the cost function [20]. The individuals are represented by string of coded unknowns, each element of which is called *gene*. An hybrid integer-real coding scheme is considered. A binary encoding [21] is used for the parameters characterizing the crack. On the contrary, electric field unknowns are represented with real-valued genes [22], [8]. Then the following sequence of steps is performed:

- Randomly generate an initial population, $\Omega^{(0)}$;
- Compute the value of the cost function of each individual of the current population, $\underline{\xi}_l^{(k)}$ being k the population number;
- Generate an intermediate population, $\Omega_{int}^{(k)}$, applying the *proportionate selection* [6] operator;
- Generate a new population, $\Omega^{(k+1)}$, applying *mutation* and *crossover* operators to $\Omega_{int}^{(k)}$. These operators are applied in probability, where the crossover and mutation probabilities are system parameters. As far as crossover operator is concerned standard *two-point crossover* is used [7]. The mutation is performed following different strategies according to the type of the gene to mutate. If the randomly selected gene is binary-valued, then standard *binary mutation* is adopted. Otherwise, the gene is modified by adding a random value, such that the obtained solution be physically admissible.

- When L_Ω new individuals are generated, the *elitism* mechanism [5] is applied in order to always maintain the best solution in the current population.

The iterative procedure is repeated until a termination criterion is attained. In particular, the process is stopped if a fixed threshold for the value of the cost function (ζ) is attained or if a maximum number of generations is achieved (K_{max}).

3 Numerical Results

To test the performance of the proposed algorithm, a number of simulations have been performed with the use of both noiseless and noisy synthetic data. Let us consider a lossy square host object $0.8\lambda_0$-sided, being λ_0 the free-space wavelength, characterized by a relative dielectric permittivity $\varepsilon_{object}(x, y) = 2.0$. The scatterer is successively illuminated by $V = 4$ incident unit plane waves whose impinging directions are given by $\vartheta_v = (v-1)\frac{2\pi}{V}$, $v = 1, ..., V$. The observation domain is made up of $M = 40$ measurement points equally spaced and located in a circle $0.64\lambda_0$ in radius.

In the first example, the effect of the conductivity of the host medium on the detection of a crack is analyzed. A square crack ($L = W = 0.2\lambda_0$) is centered at the point $x_0 = y_0 = 0.1\lambda_0$. The assumed parameter concerning the GA (chosen according to values suggested in the literature [6], [7]) are the following: crossover probability, $p_c = 0.7$; mutation probability, $p_m = 0.7$; dimension of the population, $L_\Omega = 80$; maximum number of generations, $K_{max} = 1000$; cost function threshold, $\zeta = 10^{-5}$.

In order to quantify the errors in the crack positioning, in the definition of the crack area, and for the electric field prediction suitable error figures are defined:

$$\gamma_c = \frac{\sqrt{(x_0 - \widehat{x}_0)^2 + (y_0 - \widehat{y}_0)^2}}{d_{max}} \times 100 \quad (location\ error) \tag{3}$$

$$\gamma_A = \frac{A_c - \widehat{A}_c}{A_c} \times 100 \quad (area\ error) \tag{4}$$

$$\Phi_n = \frac{\left|\left|\widehat{E}_{tot}^{v,n}\right| - \left|E_{tot}^{v,n}\right|\right|}{\left|E_{tot}^{v,n}\right|} \times 100 \quad (field\ error) \tag{5}$$

being $(\widehat{x}_0, \widehat{y}_0)$ the estimated coordinates of the crack, $d_{max} = \sqrt{2} l_D$ the maximum error in defining the crack center when it belongs to the host scatterer, $\widehat{A}_c$ and A_c the estimated and actual crack areas, respectively, and $\widehat{E}_{tot}^{v,n}$ the estimated electric field inside the nth subdomain. Figure 2, shows the behavior of the maximum, average and minimum values of the location (Fig. $2(a)$) and area (Fig. $2(b)$) errors versus σ. As can be seen, the algorithm performs better in the crack location than in defining the crack dimensions. As far as the location error is concerned, the average value is less than 13% in the range of variability of σ. On the contrary, the area error results less than 50% for a conductivity value ranging between 0 and 0.4 (S/m), and considerably increases for larger value of σ. For completeness, Figure 3 shows the plots of the electric field distribution ($\nu = 3$) inside the investigation domain when $\sigma = 0.3$ (S/m). In more detail, figures $3(a)$ and $3(b)$ give the field amplitude for the crack-free configuration and for the reference configuration with the crack, respectively. In order to give some indications about the convergence of the iterative procedure, figures $3(c)$-$3(f)$ show the plot of Φ_n inside the investigation domain for different iterations. Starting from the initial iteration ($k = 0$), the average value of the field error decreases until a percentage value equal to 26% is reached at the stopping iteration ($k = 1000$) (Table I).

An idea of the data fitting obtained with the presented approach is given in Figure 4 and Figure 5. Figure 4 shows the amplitude of the estimated scattered electric field ($\nu = 3$) in the observation domain. The reconstructed amplitudes are given in correspondence with different iterations and also the actual distribution is reported. Starting from the iterations around $k = 400$, the agreement between reference and reconstructed amplitudes is very good. For completeness, the fitness function and related addends (i.e., $\phi_{Data}\left\{\underline{\xi}\right\} = \sum_{m=1}^{M}\sum_{v=1}^{V}\left|E_{scatt}^{v,m} - \Im^{v,m}\left\{\underline{\xi}\right\}\right|^2$ and $\phi_{State}\left\{\underline{\xi}\right\} = \sum_{n=1}^{M}\sum_{v=1}^{V}\left|E_{inc}^{v,m} - \Im_0^{v,n}\left\{\underline{\xi}\right\}\right|$) are shown in Figure 5. The plots confirm a good fitting with the data related to the scattered electric

field in the observation domain as well as with those proportional to the incident field inside the investigation domain.

The results in a noisy environment are considered in the second example where the host medium is characterized by a conductivity $\sigma = 0.1$ (S/m). To simulate the presence of the noise in observed data, Gaussian noise is added. The noise is a complex random variable whose real and imaginary parts are independent Gaussian random variables with zero mean and standard deviation given by

$$\sigma = \frac{\sum_{n=1}^{M} \sum_{v=1}^{V} \left| \widehat{E}_{scatt}^{v,m} \right|^2}{2NV \left(\frac{S}{N} \right)} \tag{6}$$

being $\left(\frac{S}{N}\right)$ the signal-to-noise ratio. The results in term of error figures, derived from the inversion procedure when a Gaussian noise characterized by different power levels is considered, are given in Table II. The influence of the noise on the reconstruction capabilities of the approach is visible. The values of the error figures increase as the signal-to-noise ratio decreases. However it should be noted that the approach show a good robustness to the noise. As far as γ_c and γ_A are concerned the increase in the error values results less than 5% and 7% between the strongly and weakly noisy case, respectively.

Finally, the detection of an irregular crack has been considered. Figure 6 is concerned with the case of a void crack located inside a lossy host medium ($\sigma = 0.01$(S/m)) as shown in Figure 6(a). In particular, Figures 6(b), 6(c), and 6(d) give the images of the reconstructed configuration at the initialization ($k = 0$), at an intermediate iteration ($k = 50$), and at the convergence iteration ($k^* : \phi_{k*} \left\{ \underline{\xi} \right\} < \zeta$), respectively. Starting from an initial estimate of the area and location of the crack randomly chosen (fig. 6(b)), the estimated crack parameters tend to become more and more similar to the actual one. The final image (fig. 6(d)) shows that the crack is correctly located and also the crack area is similar to the reference one. In particular, the estimate of the crack area results very good if we consider that the constraint of a rectangular crack to be detected is assumed

during the iterative process.

4 Conclusions

A two-dimensional inverse scattering method for reconstructing the parameters of a crack located inside a lossy host medium has been proposed. The method is based on minimizing the mean-square errors between measured and reconstructed scattered and incident electric fields, respectively. Unlike the inversion methods based on deterministic optimization techniques, the proposed approach allows to use the large amount of *a-priori* knowledge avoiding the solution to be trapped in local minima of the nonlinear functional.

The reconstruction technique has been tested with synthetic data in both noisy and noiseless conditions. It has been demonstrated that quite accurate results can be achieved especially as far as the crack location is concerned.

Finally, preliminary results concerned with an irregular void crack have been shown. Further improvement in the performance of the proposed approach may be achieved by adding appropriate penalty terms or by choosing a more accurate parameterization of the crack perimeter. This is left for future works.

References

[1] M. Pastorino, *IEEE Trans. Instrum. Meas.* **47** (1998), 1419-1427.

[2] R. C. Popa and K. Miya, *J. Nondestr. Eval.* **17** (1998), 209-221.

[3] D. Lesselier and A. Razek, *Electromagnetic Nondestructive Evaluation (III)*, IOS Press, Amsterdam, 1999.

[4] P. Ramuhalli, M. Azfal, K. T. Hwang, S. Udpa, and L. Udpa, in: *Electromagnetic Nondestructive Evaluation (IV)*, S. S. Upda et al., eds., IOS Press, Amsterdam, 2000, pp. 1-8.

[5] D. E. Goldberg, *Genetic Algorithms in Search, Optimization and Machine Learning,* Addison-Wesley, Reading MA, 1989.

[6] J. M. Johnson and Y. Rahmat-Samii, *IEEE Trans. Antennas Propagat. Magaz.* **39** (1997), 7-25.

[7] D. S. Wiele and E. Michielssen, *IEEE Trans. Antennas Propagat.* **45** (1997), 343-353.

[8] S. Caorsi, A. Massa, and M. Pastorino, *IEEE Trans. Geosci. Remote Sensing* **38** (2000), 1697-1708.

[9] S. Y. Yang, L. J. Park, C. H. Park, and J. W. Ra, in: *Proc. IEEE Inter. Conf. on Evolutionary Computation*, 1995, pp. 450-455.

[10] F. Xiao and H. Yabe, *IECE Trans. Electron.* **E81-c** (1998), 1784-1792.

[11] F. Zaoui, C. Marchand, and J. Pavo, in: *Proc. 6th Int. Workshop on Electromagnetic Nondestructive Evaluation* (ENDE 2000), Budapest, Hungary, 2000, pp. 49-50.

[12] F. Zaoui, C. Marchand, and A. Razek, in: *Proc. 4th Int. Workshop on Electromagnetic Nondestructive Evaluation* (ENDE'98), Chatou, France, 1998, pp. 26-27.

[13] R. Albanese, G. Rubinacci, A. Tamburrino, and F. Villone, in: *Proc. Int. Symp. on Non-linear EM Systems* (ISEM 1999), Pavia, Italy, 1999, pp. 105.

[14] H. L. M. dos Reis, A. C. Voegele, and D. B. Cook, in: *Nondestructive Characterization of Materials IX.* R. E. Green, ed., AIP, New York, 1999, pp. 33-40.

[15] D. Ioan, M. Rebican, and A. Duca, in: *Proc. 6th Int. Workshop on Electromagnetic Nondestructive Evaluation* (ENDE 2000), Budapest, Hungary, 2000, pp. 17-18.

[16] D. S. Jones, *The Theory of Electromagnetism,* Pergamon Press, Oxford, 1964.

[17] S. Caorsi, G. L. Gragnani, and M. Pastorino, *IEEE Trans. Microwave Theory Tech.* **39** (1991), 845-851.

[18] M. Idemen, *Inverse Probl.* **5** (1989), 1057-1074.

[19] M. Slaney, A. C. Kak, and L. E. Larsen, *IEEE Trans. Microwave Theory Tech.* **32** (1984), 861-873.

[20] G. Rudolph, *IEEE Trans. Neural Networks* **5** (1994), 96-101.

[21] J. H. Holland, *Adaption in Natural and Artificial Systems*, Univ. of Michigan Press, Ann Arbor, 1975.

[22] D. E. Goldberg, *Complex Systems* **5** (1991), 139-167.

FIGURE CAPTIONS

- Figure 1.

  Problem Geometry.

- Figure 2.

  Reconstruction of a void crack inside a lossy host medium. Minimum, maximum, and average values of (a) γ_c and of (b) γ_A for different values of the host medium conductivity.

- Figure 3.

  Reconstruction of a void crack inside a lossy host medium ($\sigma = 0.3$ (S/m)). Amplitude of the electric field inside the investigation domain ($\nu = 3$). (a) Crack-free distribution. (b) Actual distribution. Field error distribution inside the investigation domain obtained by using the microwave imaging approach at the iterations (c) $k = 0$, (c) $k = 100$, (c) $k = 500$, and (c) $k = 1000$.

- Figure 4.

  Reconstruction of a void crack inside a lossy host medium ($\sigma = 0.3$ (S/m)). Amplitude of the scattered electric field at the measurement points ($\nu = 3$). Comparison between actual and reconstructed values.

- Figure 5.

  Reconstruction of a void crack inside a lossy host medium ($\sigma = 0.3$ (S/m)). Behavior of the functional versus the number of iterations.

- Figure 6.

  Reconstruction of a void irregular crack inside a lossy host medium ($\sigma = 0.01$ (S/m)). Images of reconstruction results. (a) Actual configuration. Reconstructed configuration at the iterations (b) $k = 0$, (c) $k = 50$, and (d) $k = 1000$.

TABLE CAPTIONS

- Table I.

  Reconstruction of a void crack inside a lossy host medium ($\sigma = 0.3$ (S/m)). Statistics of the field error inside the investigation domain for different numbers of iterations. Simulation in Fig. 3.

- Table II.

  Influence of the noise on the reconstruction of a void crack inside a lossy host medium ($\sigma = 0.01$ (S/m)). Error figures.

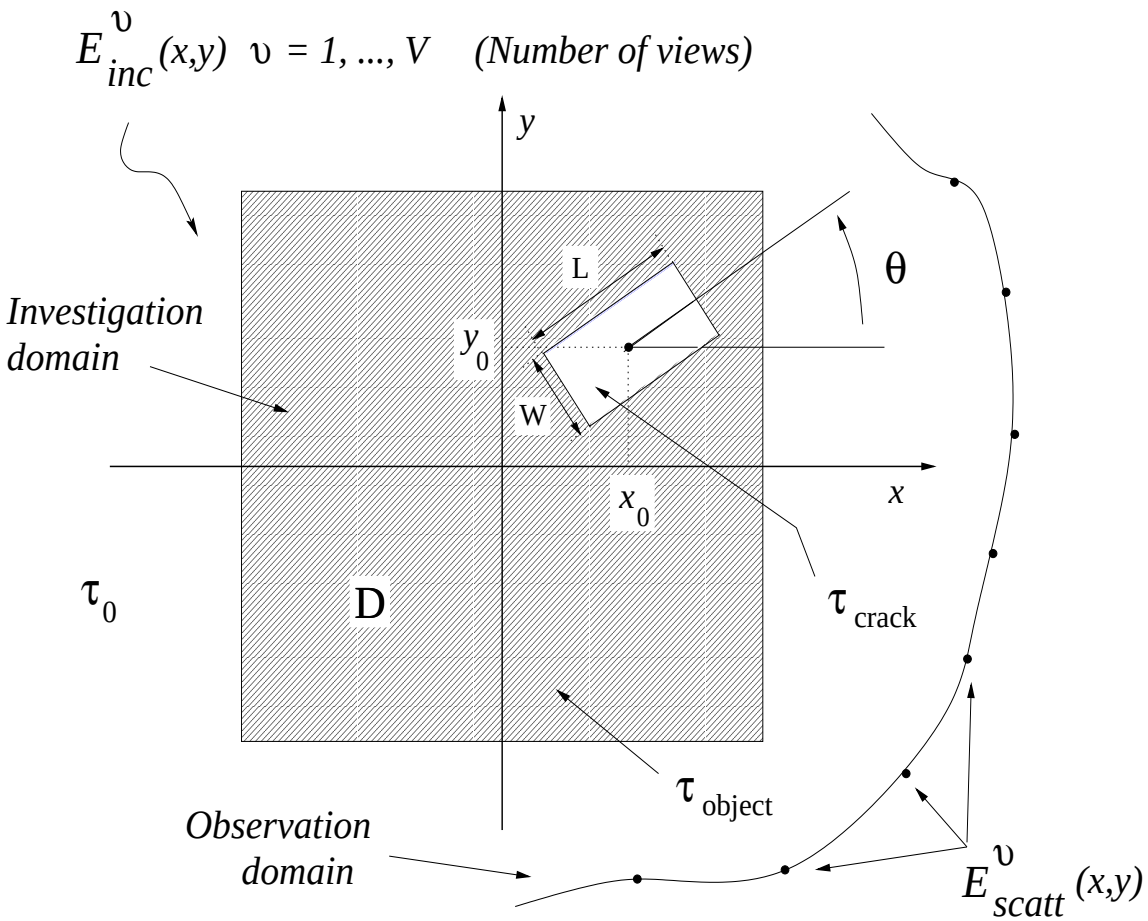

Fig. 1 - S. Caorsi et al., "Crack Detection in Lossy ..."

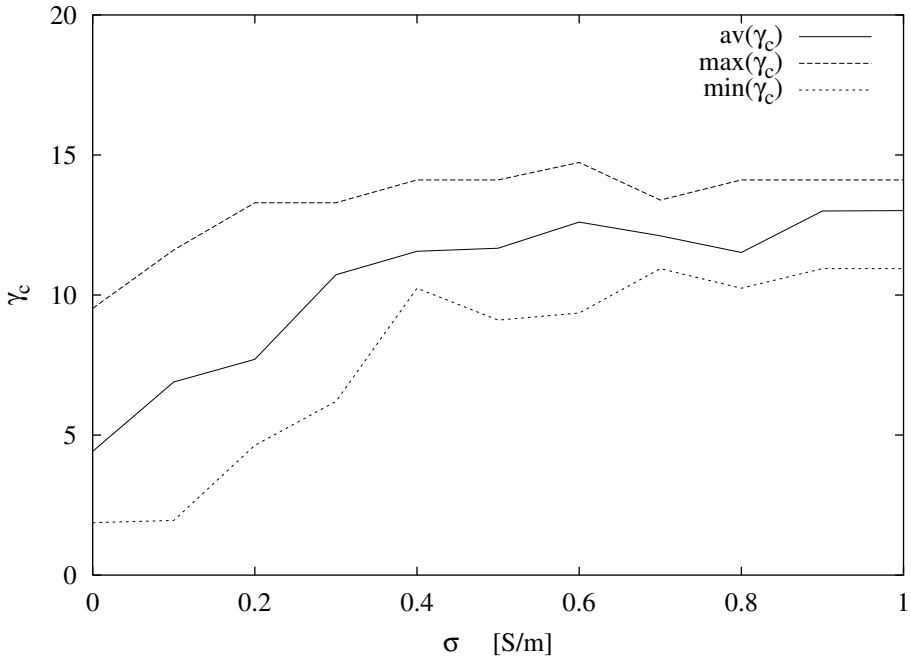

(a)

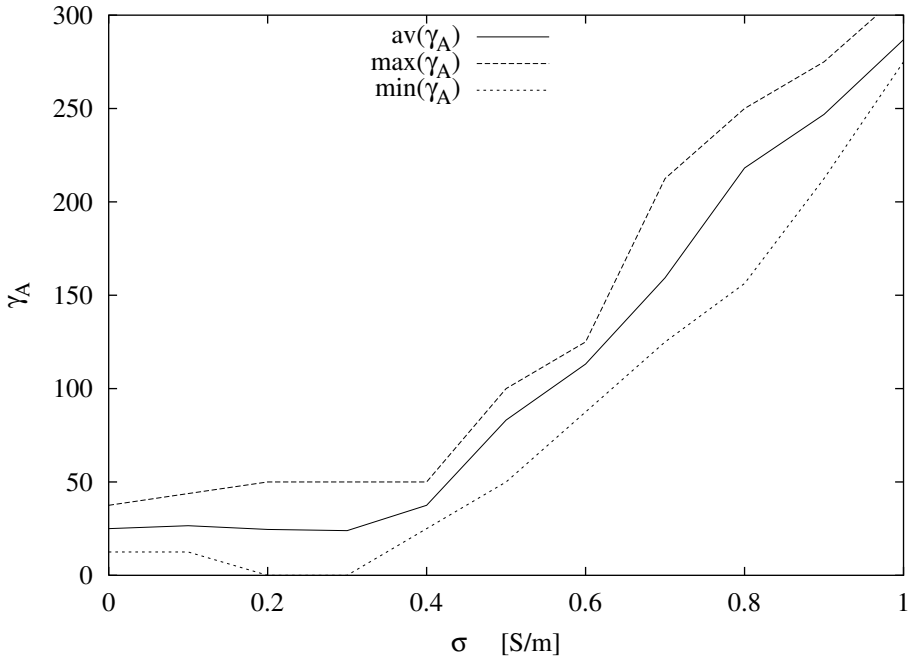

(b)

Fig. 2 - S. Caorsi et al., "Crack Detection in Lossy ..."

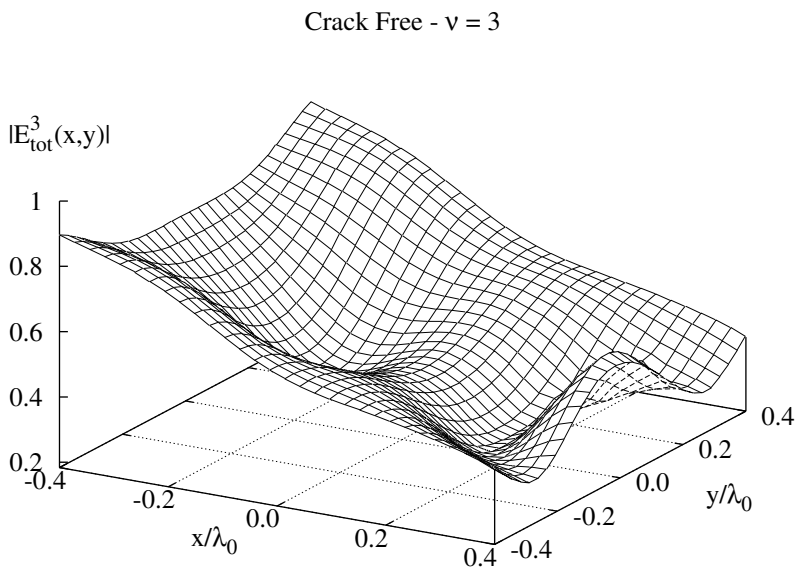

(a)

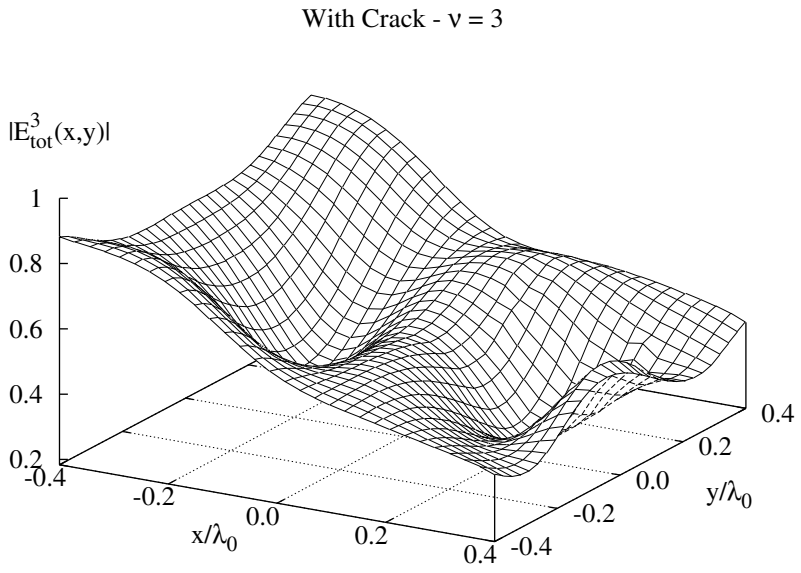

(b)

Fig. 3 - S. Caorsi et al., "Crack Detection in Lossy ..."

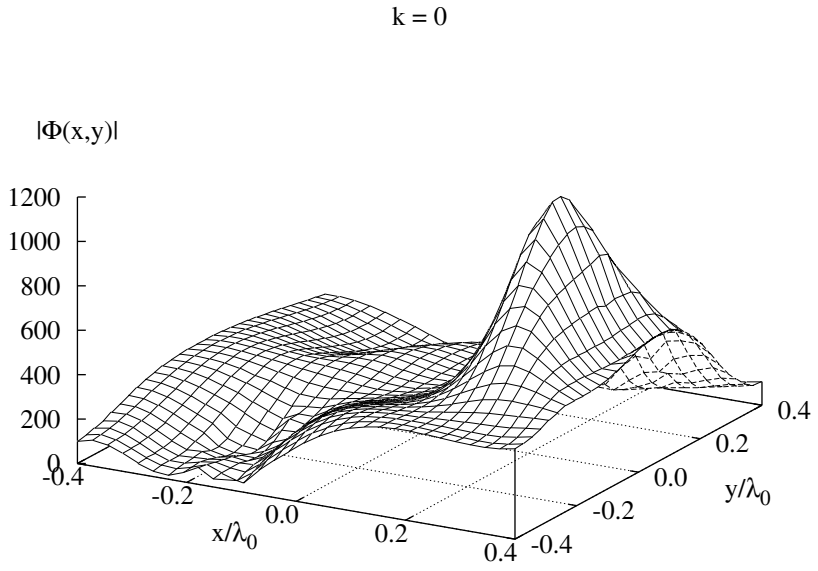

(c)

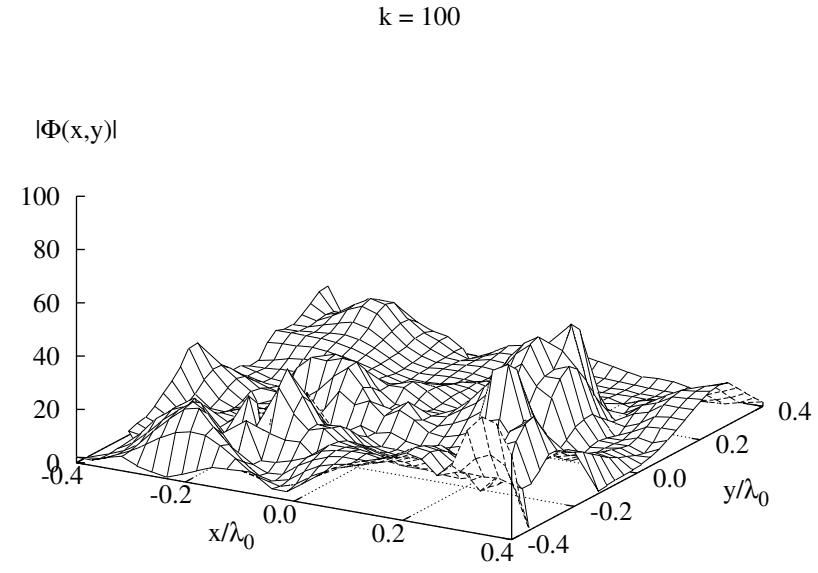

(d)

Fig. 3 - S. Caorsi et al., "Crack Detection in Lossy ..."

k = 500

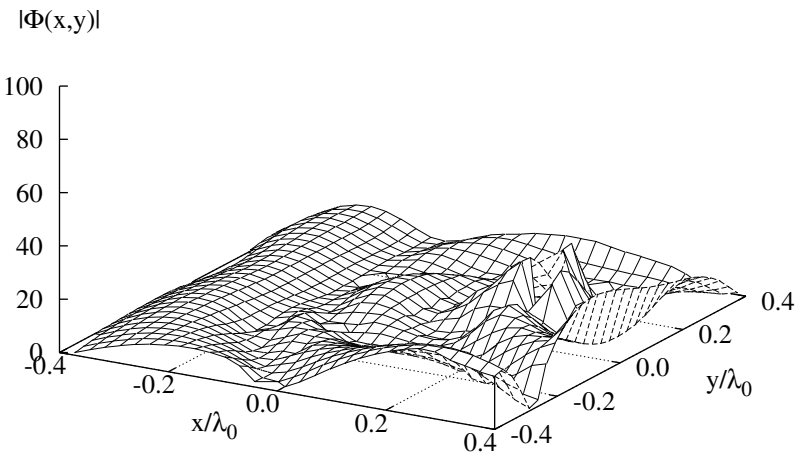

(*e*)

k = 1000

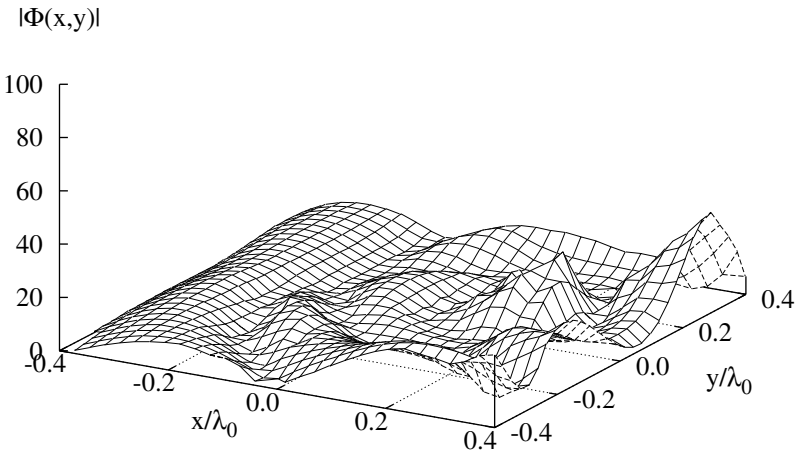

(*f*)

Fig. 3 - S. Caorsi et al., "Crack Detection in Lossy ..."

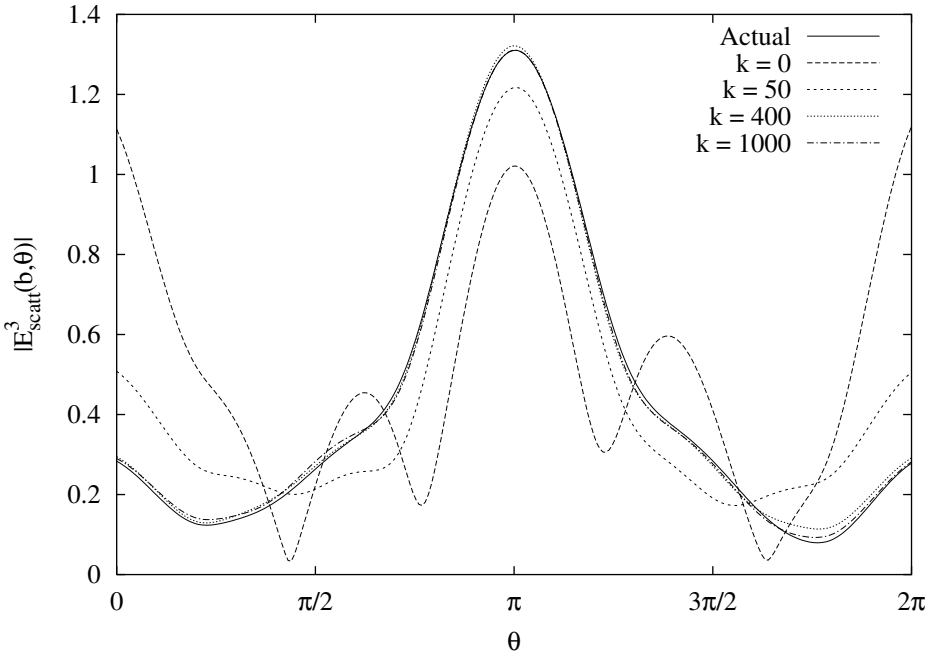

Fig. 4 - S. Caorsi et al., "Crack Detection in Lossy ..."

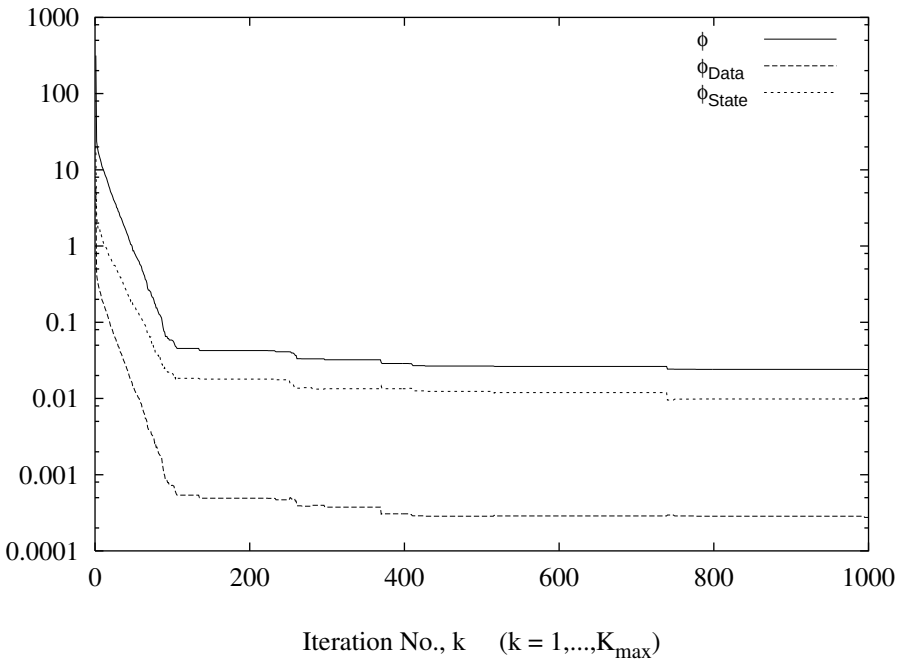

Fig. 5 - S. Caorsi et al., "Crack Detection in Lossy ..."

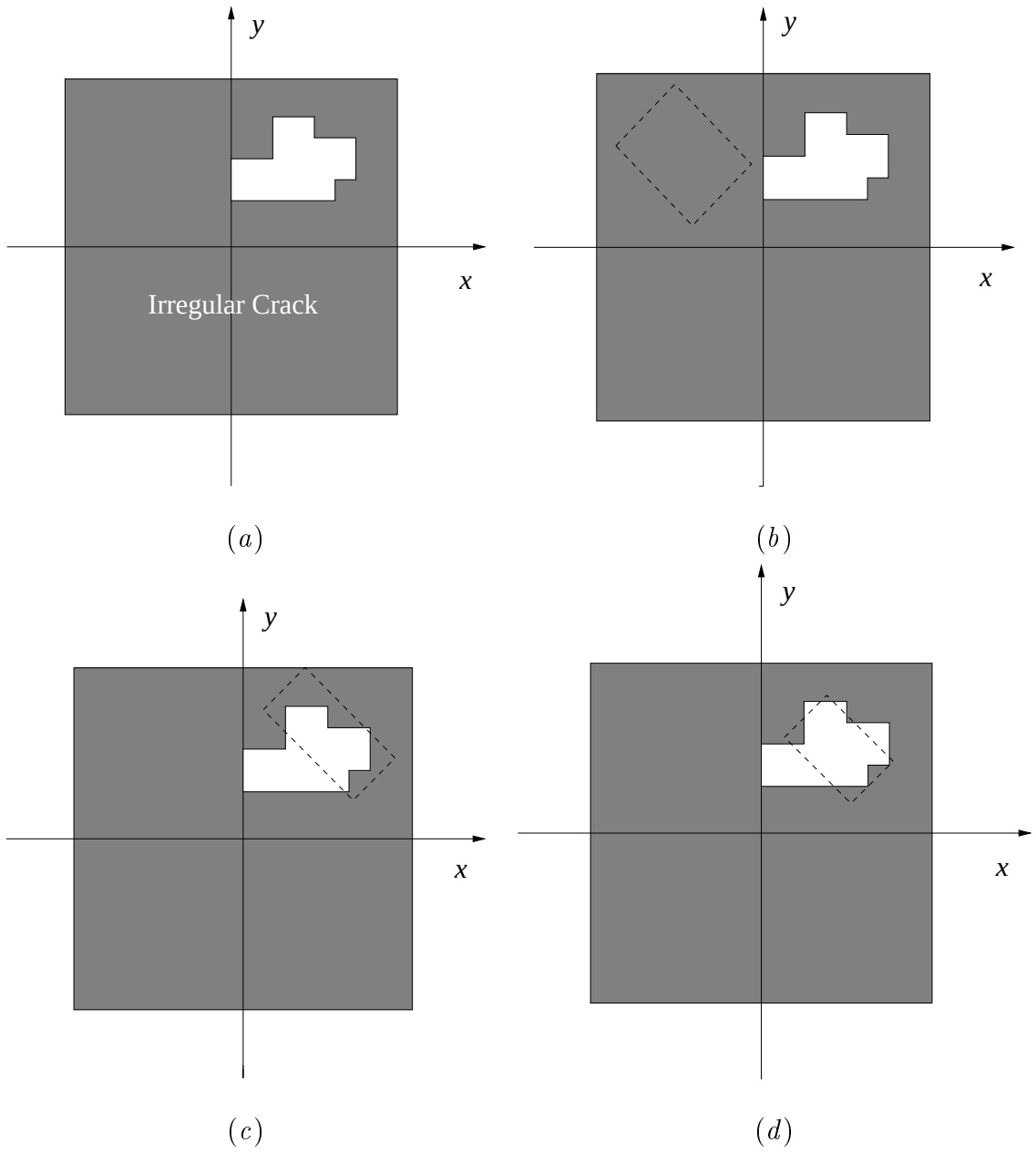

Fig. 6 - S. Caorsi et al., "Crack Detection in Lossy ..."

k	$av\{\Phi(x,y)\}$	$var\{\Phi(x,y)\}$	$min\{\Phi(x,y)\}$	$max\{\Phi(x,y)\}$
0	365.40	4519.4	0.29×10^{-1}	1138.44
100	15.47	64.47	0.36×10^{-2}	43.95
500	12.61	29.66	0.26×10^{-1}	29.65
1000	12.10	26.00	0.66×10^{-2}	31.85

Tab. I - S. Caorsi et al., "Crack Detection in Lossy ..."

$\left(\frac{S}{N}\right)_{dB}$	γ_c	γ_A	$av\left\{\Phi\left(x,y\right)\right\}$
10	9.53	49.37	12.664
30	7.38	47.11	12.614
50	4.92	42.96	12.613

Tab. II - S. Caorsi et al., "Crack Detection in Lossy ..."